Published online 6 May 2011 *Nucleic Acids Research, 2011, Vol. 39, No. 15* ***6825–6834***
doi:10.1093/nar/gkr281

Highly fluorescent guanosine mimics for folding and energy transfer studies

Anaëlle Dumas and Nathan W. Luedtke*

Institute of Organic Chemistry, University of Zürich, Winterthurerstrasse 190, CH-8057 Zürich, Switzerland

Received February 20, 2011; Revised April 11, 2011; Accepted April 12, 2011

ABSTRACT

Guanosines with substituents at the 8-position can provide useful fluorescent probes that effectively mimic guanine residues even in highly demanding model systems such as polymorphic G-quadruplexes and duplex DNA. Here, we report the synthesis and photophysical properties of a small family of 8-substituted-2′-deoxyguanosines that have been incorporated into the human telomeric repeat sequence using phosphoramidite chemistry. These include 8-(2-pyridyl)-2′-deoxyguanosine (2PyG), 8-(2-phenylethenyl)-2′-deoxyguanosine (StG) and 8-[2-(pyrid-4-yl)-ethenyl]-2′-deoxyguanosine (4PVG). On DNA folding and stability, 8-substituted guanosines can exhibit context-dependent effects but were better tolerated by G-quadruplex and duplex structures than pyrimidine mismatches. In contrast to previously reported fluorescent guanine analogs, 8-substituted guanosines exhibit similar or even higher quantum yields upon their incorporation into nucleic acids ($\Phi = 0.02–0.45$). We have used these highly emissive probes to quantify energy transfer efficiencies from unmodified DNA nucleobases to 8-substituted guanosines. The resulting DNA-to-probe energy transfer efficiencies (η_t) are highly structure selective, with η_t(duplex) < η_t(single-strand) < η_t(G-quadruplex). These trends were independent of the exact structural features and thermal stabilities of the G-quadruplexes or duplexes containing them. The combination of efficient energy transfer, high probe quantum yield, and high molar extinction coefficient of the DNA provides a highly sensitive and reliable readout of G-quadruplex formation even in highly diluted sample solutions of 0.25 nM.

INTRODUCTION

From the early days of structural biology, DNA was recognized as having the ability to adopt alternate folds (1). In addition to A-, B- and Z-form double helices, DNA can fold into a variety of hairpin, triplex, G-quadruplex and i-motif structures that contain non-canonical base pairs (2,3). While the exact biological relevance of these structures remains an open question, DNA sequences with the ability to fold into G-quadruplex structures have been implicated in regulating gene transcription (4–6), recombination (7), chromosome stability (8–10) and programmed cell death (11). In all cases, open questions still remain about the exact folding pathways and biologically active conformation(s) of these DNA sequences (12).

A wide variety of biophysical techniques have been used to characterize DNA folding *in vitro*. These include NMR (13–15), circular dichroism (CD) (16), UV absorption (17,18), X-ray crystallography (19), FRET (20–22) and immunostaining (23). Most of these methods require pure DNA samples and are not compatible with conformational analyses in living cells. While fluorescence spectroscopy has the potential for conformational analyses *in vivo*, techniques involving high-affinity fluorescent probes or DNA molecules conjugated to large fluorescent tags can perturb the structure and/or stability of the DNA itself (21,24,25). Further development of fluorescence-based methods is needed to provide highly sensitive, non-perturbing tools to characterize DNA folding *in vitro* and *in vivo*. Due to their small size and predictable location, internal fluorescent probes offer some advantages over linker-attached chromophores, such as the ability to report subtle structural changes with single nucleotide resolution (26–29).

Modification of the 8-position of guanosine is an attractive avenue to fluorescent derivatives because it is not directly involved in base-pairing interactions within G-quadruplex or duplex structures (R^2, Figure 1A). Derivatization of this position can generate fluorescent products (Figure 1B) (30–34) with emission properties

*To whom correspondence should be addressed. Tel: +41 44 635 4244; Fax: +41 44 635 6891; Email: luedtke@oci.uzh.ch

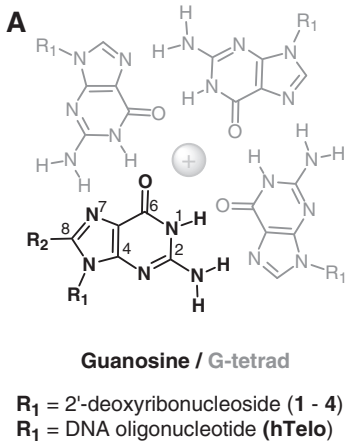

B

Entry	R_2	λ_{abs} / λ_{em}(nm)	Φ (CH_3CN)	Φ (H_2O)	Φ (D_2O)
"dG" (1)	H–	260 / 330	n.d	$< 10^{-4}$	n.d
"2PyG" (2)		300 / 415	0.71	0.02	0.04
"StG" (3)		340 / 450	0.74	0.49	0.50
"4PVG" (4)		355 / 490	0.57	0.16	0.30

Figure 1. (**A**) Structures and numbering of 8-substituted-2′-deoxyguanosines and an ion-containing G-tetrad (gray). (**B**) Wavelengths of maximal absorbance (λ_{abs}) and emission (λ_{em}) in water, and quantum yield (Φ) of each nucleoside in acetonitrile, water or D_2O.

that are sensitive to DNA folding (34). While the addition of bulky groups to the 8-position of guanosine can shift the conformational equilibrium of the glycosidic bond from '*anti*' to '*syn*' (35–38), DNA folding can force 8-modified guanosines to adopt *anti* conformations with relatively small energetic penalties to DNA folding ($\Delta\Delta G \leq 1\,kcal\,mol^{-1}$) (37,38).

We recently reported 8-(2-pyridyl)-2′-deoxyguanosine '**2PyG**' (Entry 2, Figure 1B) as a 'turn-on' fluorescence probe of G-quadruplex folding and energy transfer (34). Upon its incorporation into G-tetrads, **2PyG** was minimally disruptive to intramolecular G-quadruplex folding where it exhibited higher quantum yields (Φ = 0.04–0.15) than the corresponding nucleoside (**2**) in water (Φ = 0.02). Using **2PyG**, we discovered efficient energy transfer reactions involving unmodified guanosines in G-quadruplex structures (DNA-to-probe energy transfer efficiency, η_t = 0.11–0.41) that depended on the presence and identities of cations coordinated to the O^6 positions of the guanine residues. It was unclear from these studies, however, if the reported intramolecular energy transfer reactions resulted from unusual intrinsic properties of G-quadruplexes, the unusual photophysical characteristics of **2PyG**, or some combination thereof. To help address this question, we have synthesized oligonucleotides containing 8-(2-phenylethenyl)-2′-deoxyguanosine (**StG**) and 8-[2-(pyrid-4-yl)-ethenyl]-2′-deoxyguanosine (**4PVG**, Figure 1B) and evaluated their ability to report DNA folding and internal energy transfer reactions in G-quadruplex, single-stranded and duplex structures derived from the human telomeric repeat sequence. As compared to **2PyG**, both of the vinyl-bridged derivatives **4PVG** and **StG** exhibit red-shifted excitation and emission maxima, lower potentials for perturbing DNA structure, and higher quantum yields (Φ = 0.03–0.44) in the context of folded DNA. For all three 8-substituted guanosines, DNA-to-probe energy transfer efficiencies were much higher in G-quadruplex structures (η_t = 0.12–0.30) than the same oligonucleotides folded into B-form duplexes (η_t = 0.02–0.06). The unusual photophysical properties of cation-containing G-quadruplexes are therefore responsible for the efficient energy transfer reactions within these structures (34). These phenomena together provide a reliable and highly sensitive means for deciphering the folded state of the DNA (duplex versus quadruplex) even in highly diluted sample solutions of ≤250 pM.

MATERIALS AND METHODS

Synthesis of 8-substituted-2′-deoxyguanosine nucleosides and phosphoramidites

The **2PyG** nucleoside (**2**) and corresponding β-cyanoethyl phosphoramidite were synthesized according to published procedures (34). The phosphoramidites of 8-(2-phenylethenyl)- and 8-[2-(pyrid-4-yl)-ethenyl]-2′-deoxyguanosine were synthesized according to Scheme 1. The 8-bromo-O^6-protected-2′-deoxyguanosine derivative **6** is a highly versatile intermediate for palladium catalyzed cross-coupling reactions including Suzuki, Stille and Heck. The 8-(2-phenylethenyl)-derivative **7** was synthesized by Suzuki–Miyaura cross-coupling of **6** with commercially available *trans*-styryl boronic acid pinacol ester to yield the *trans* isomer of **7**. The analogous pyridine derivative **9**, was made by first preparing the vinyl derivative **8** *via* Stille coupling of **6** with tributyl(vinyl) tin, followed by addition of the pyridine group via Heck coupling. The resulting *trans* derivatives **7** and **9** were deprotected with tetrabutylammonium fluoride (TBAF) to furnish free nucleosides (**3** and **4**, Figure 1B), or they were carried forward into phosphoramidite synthesis using standard methodologies for N(2) protection with isobutyryl chloride (**10** and **11**), followed by deprotection with TBAF (**12** and **13**) and the addition of dimethoxytrityl to the 5′OH groups (**14** and **15**). The detailed synthetic procedures and characterization of these intermediates are available in the supporting information. Slightly different procedures were needed for introducing the cyanoethyl phosphoramidite on the 3′OH of each compound (**16** and **17**). In the case of **17**, a base

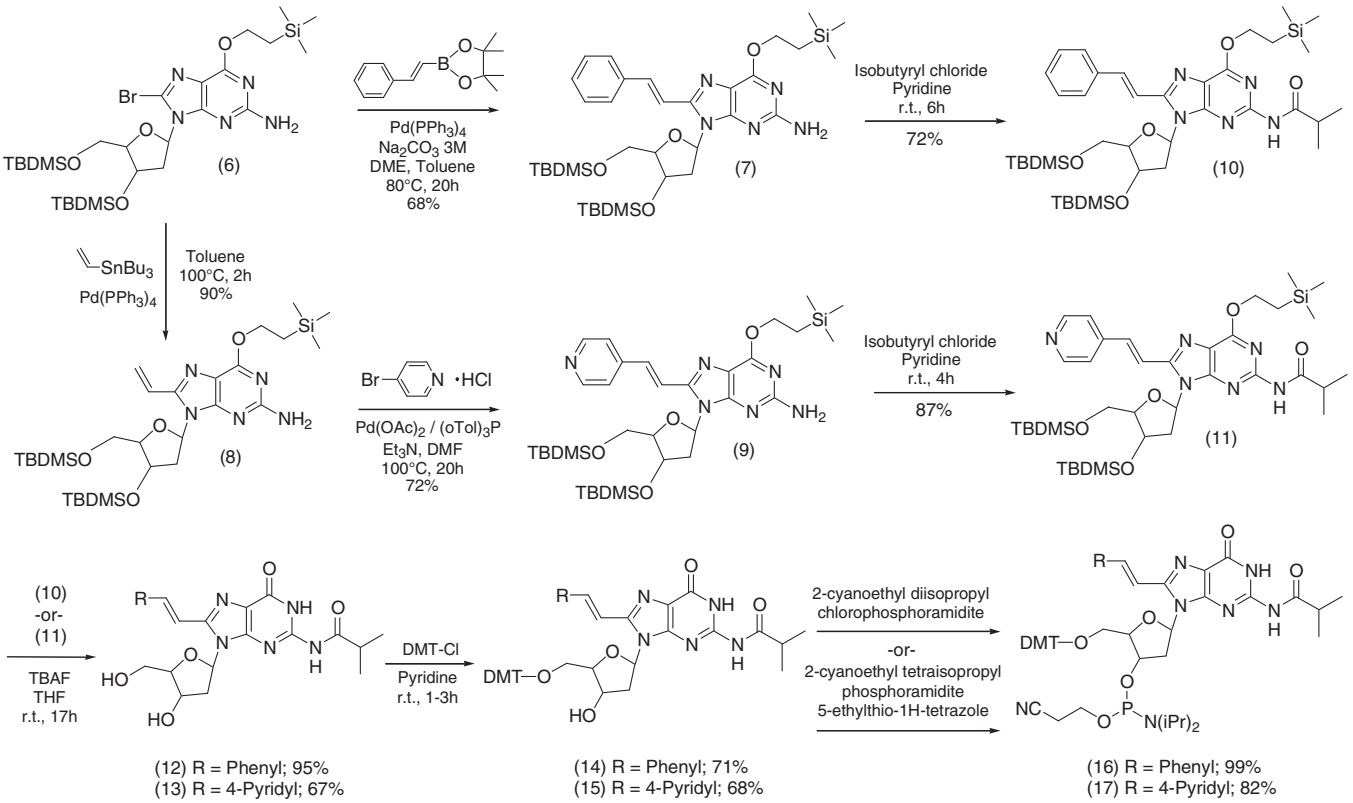

Scheme 1. Synthesis of the 8-(substituted)-2′-deoxyguanosine phosphoramidites **16** and **17**.

catalyzed reaction with 2-cyanoethyl diisopropylchloro phosphoramidite was successful, while compound **16** was prepared by an acid catalyzed reaction of **14** with 2-cyanoethyl tetraisopropyl phosphordiamidite by 5-ethylthio-(1 *H*)-tetrazole. All new compounds were characterized by NMR and mass spectrometry (Supplementary Data), except for compound **16** that was carried directly into oligonucleotide synthesis without isolation (39).

Oligonucleotide synthesis

Modified oligonucleotides were synthesized on a 1-μmol scale using a Millipore Expedite 8909 DNA synthesizer according to the standard Trityl-off procedure, except that 5% dichloroacetic acid in CH_2Cl_2 was used for Trityl deprotection. Manual coupling reactions were used for the site-specific introduction of **16** and **17** into oligonucleotides. These phosphoramidites (0.02 mmoles) were dissolved into 200 μl of 0.25 M 5-ethylthio-(1 *H*)-tetrazole in dry acetonitrile and added to DNA columns via syringe for 10 min. Upon completion of each sequence, oligonucleotides were cleaved from the solid support and deprotected by treatment with 1.5 ml of 33% aqueous ammonium hydroxide at 55°C for 17 h in a 1.7-ml screw-top cap tube. The resulting products were dried, dissolved into water and purified by using C-18 reversed phase HPLC with a mobile phase of 0.1 M triethyl ammonium acetate (pH 7) and acetonitrile. Following lyophilization, oligonucleotide stock solutions were prepared in pure water and quantified using $\varepsilon_{(260\ nm)} = 244\,300\ cm^{-1}M^{-1}$. MALDI-TOF MS hTeloG9: G9 = **StG** (*m*/*z*) calcd, 7676.4; found 7684.5; G9 = **4PVG** (*m*/*z*) calcd, 7677.4; found 7680.4; hTeloG23: G23 = **StG** (*m*/*z*) calcd, 7676.4; found 7678.4; G23 = **4PVG** (*m*/*z*) calcd, 7677.4; found 7677.8. The synthesis and characterization of the **2PyG**-containing oligonucleotides were reported elsewhere (34). See Supplementary Figures S1–S6 for analytical HPLC chromatograms and MALDI-MS spectra.

DNA folding and buffer conditions

Duplex DNA samples were prepared in the presence of 100 mM NaCl and 1.1 equivalents of the complementary strand. G-quadruplex structures were prepared from single-stranded oligonucleotides in 100 mM of NaCl or KCl-containing buffers. Unfolded, single-stranded DNAs were prepared in 100 mM LiCl. Buffers were prepared as 10 mM cacodylic acid solutions containing the indicated salt, and the pH was adjusted to 7.4 by neutralization with KOH, NaOH or LiOH. The final buffers had the following compositions: (K^+): 10 mM potassium cacodylate buffer + 100 mM KCl; (Na^+): 10 mM sodium cacodylate buffer + 100 mM NaCl; (Li^+): 10 mM lithium cacodylate buffer + 100 mM LiCl; duplex sample (DS): 10 mM sodium cacodylate buffer + 100 mM NaCl. Oligonucleotides were diluted into buffer to final concentration of 2 μM and heated for 5 min at 95°C, and slowly cooled to room temperature overnight before use.

CD and thermal denaturation studies

CD spectra were collected on a Jasco model J-715 spectropolarimeter equipped with a Julabo FS 18 temperature control system and a 1.0-cm path length thermo-controlled CD quartz cell. Spectra were collected at 25°C between 220 and 400 nm with 0.1 nm steps, 2 nm band width and scanning rate of 50 nm min^{-1}. Three scans were averaged for each reported spectrum. For DNA-melting experiments, 2 μM solutions of pre-folded DNA were equilibrated for 15 min at 10°C and slowly ramped to 95°C at a rate of 30°C h^{-1}. The ellipticity of each sample was monitored at 290 nm for the hTelo derived G-quadruplexes and 260 nm for the corresponding duplexes. Reverse temperature scans showed no hysteresis.

Photophysical measurements

Energy transfer efficiencies and quantum yields were calculated as previously reported (34,40,41). Absorption and emission spectra were recorded using a Molecular Devices SpectraMax M5 instrument in a 1-cm path-length quartz cuvette. Instrument settings were maintained for all reported fluorescence measurements, allowing for direct comparisons of fluorescence intensities (Figure 2). For measurements of nucleoside quantum yields (Figure 1B), optical densities were adjusted to 0.1 ± 0.01 at the indicated λ_{ex} of each nucleoside and corresponding standard. As the standard for **2PyG** ($\lambda_{ex} = 300$ nm), 2-aminopyridine in 0.1 N H_2SO_4 ($\Phi = 0.6$) was used, and quinine sulfate in 0.1 M H_2SO_4 ($\Phi = 0.56$) was used as a reference for **StG** ($\lambda_{ex} = 340$ nm) and **4PVG** ($\lambda_{ex} = 355$ nm). Quantum yields of each probe in the context of oligonucleotides were determined as above except that the corresponding nucleosides in water were used as references. The excitation spectra of each probe in the context of DNA were collected using the following wavelengths of emission: 415 nm for **2PyG**, 450 nm for **StG** and 475 nm for **4PVG**. For all measurements involving oligonucleotides, 2 μM solutions of pre-folded DNA were used. This allowed for direct comparisons of CD and fluorescence spectra, but the relatively high absorbance of DNA samples at 260 nm (~0.4 AU) caused a

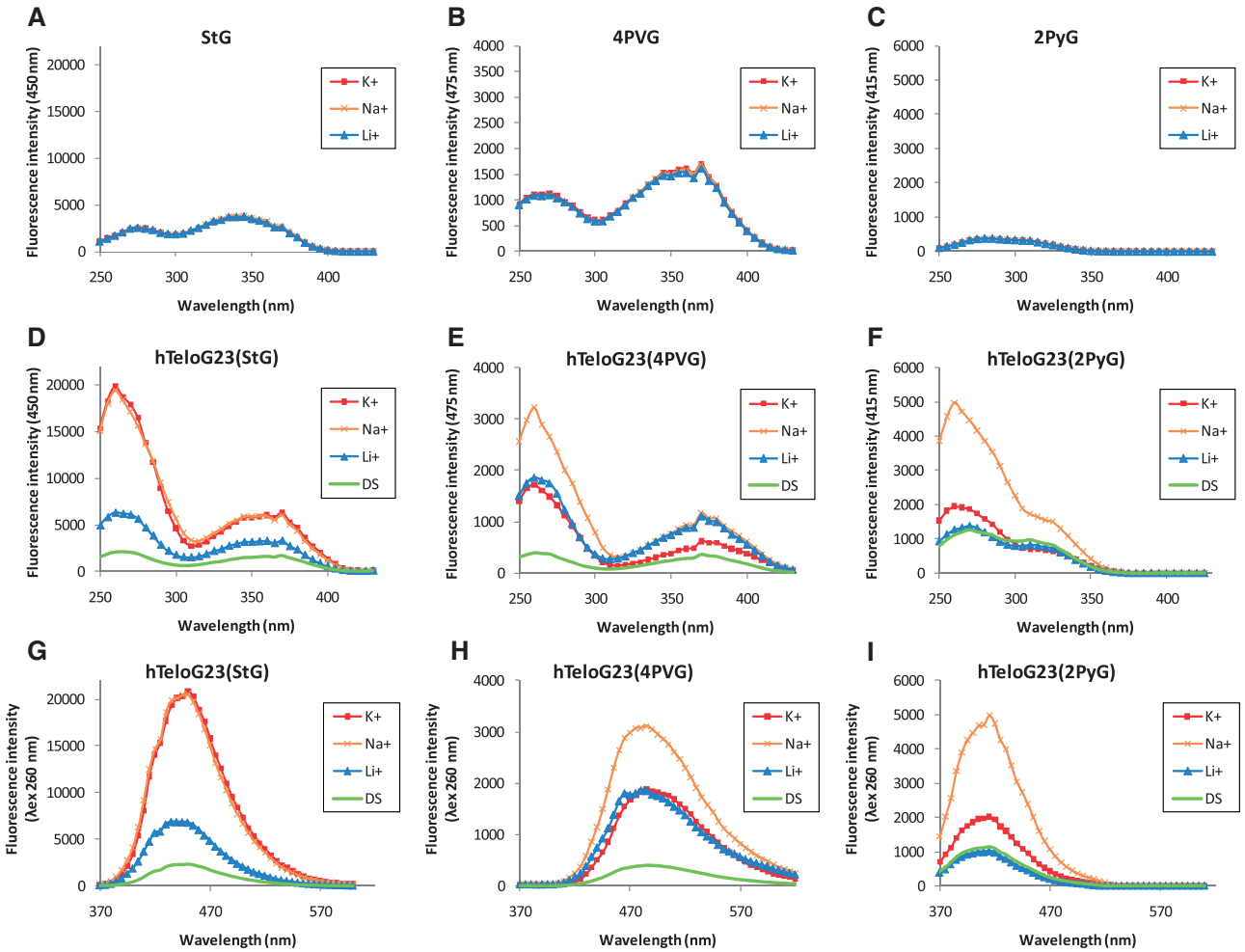

Figure 2. Excitation spectra of 2 μM of **StG** (**A**), **4PVG** (**B**) or **2PyG** (**C**) in the presence of 100 mM KCl (K^+), 100 mM NaCl (Na^+) or 100 mM LiCl (Li^+). Excitation spectra of hTeloG23(**StG**) (**D**), hTeloG23(**4PVG**) (**E**) and hTeloG23(**2PyG**) (**F**) were collected using emission at 450, 475 and 415 nm, respectively. Emission spectra of hTeloG23(**StG**) (**G**), hTeloG23(**4PVG**) (**H**) and hTeloG23(**2PyG**) (**I**) were collected using excitation at 260 nm. Double-stranded samples 'DS' included 1.1 equivalents of the complementary strand and were prepared in 100 mM NaCl. All samples contained 2 μM of DNA or 8-substituted-2′-deoxyguanosine nucleoside (**2–4**) in an aqueous 10 mM cacodylate buffer (pH 7.4).

Table 1. Quantum yield (Φ), DNA-to-probe energy transfer efficiency (η_t) and the ratio of fluorescence intensities obtained upon excitation at 260 nm [F(260)] and at 360 nm [F(360)] for **StG**, 375 nm [F(375)] for **4PVG** and 325 nm [F(325)] for **2PyG**

Name	Cond.	StG			4PVG			2PyG		
		Φ	η_t	F(260)/F(360)	Φ	η_t	F(260)/F(375)	Φ	η_t	F(260)/F(325)
hTeloG9	Li^+	0.45	0.06	2.0	0.05	0.17	2.0	0.04	0.09	2.3
	K^+	0.44	0.21	3.5	0.04	0.28	3.3	0.09	0.24	4.0
	Na^+	0.37	0.18	3.9	0.03	0.36	3.7	0.08	0.30	4.7
	DS	0.32	0.02	0.9	0.03	0.04	1.0	0.03	0.03	1.1
hTeloG23	Li^+	0.35	0.03	1.9	0.07	0.16	1.8	0.05	0.11	1.8
	K^+	0.33	0.12	3.3	0.04	0.24	2.9	0.05	0.19	3.0
	Na^+	0.37	0.12	3.3	0.06	0.31	3.0	0.10	0.26	3.3
	DS	0.20	0.02	1.3	0.02	0.05	1.2	0.04	0.06	1.4

Fluorescence spectra of these same samples are shown in Figure 2. Cond.: Measurements were performed in the presence of 100 mM KCl (K^+), 100 mM NaCl (Na^+) or 100 mM LiCl (Li^+) in an aqueous 10 mM cacodylate buffer (pH 7.4). Double-stranded samples (DS) included 1.1 equivalents of the complementary strand and 100 mM NaCl.

significant attenuation of the excitation beam that reduced the fluorescence intensities from each probe. This was evidenced by non-linear relationships between raw fluorescence intensities $F_{raw}(\lambda_{ex})$ and DNA concentrations above 50 nM when samples were photoexcited at 260 nm (Supplementary Figure S7A). $F_{raw}(\lambda_{ex})$ values at each excitation wavelength λ_{ex} were therefore corrected by multiplication with the following correction factor (CF) to obtain corrected $F(\lambda_{ex})$ values (40). Where $A(\lambda_{ex})$ is the absorbance of the sample at each wavelength of excitation.

$$CF = \frac{2.303 \times A(\lambda_{ex})}{1 - 10^{-A(\lambda_{ex})}}. \quad (1)$$

All fluorescence spectra (Figure 2) and 'F(260)/F(X)' ratios (Table 1) were measured using 2-μM solutions of DNA and corrected according to Equation (1). To check the validity of this approach, serial dilutions of **StG**-containing duplex and G-quadruplex DNAs were analyzed for fluorescence intensity as a function of sample concentration (Supplementary Figure S7). When the samples were excited at 260 nm, linear relationships were observed only after the application of the CF in Equation (1) (Supplementary Figure S7A–B). At DNA concentrations of 50 nM and below, the fluorescence intensities and $F(260)/F(X)$ ratios for the CF-corrected and uncorrected fluorescence measurements converged to the same values due to the low absorbance of the samples. These results validate the use of Equation (1). It should be emphasized that this CF is not needed for dilute DNA samples (<50 nM) having minimal optical densities (OD ≤ 0.01) at 260 nm.

RESULTS AND DISCUSSION

Cis–trans conformational analyses of nucleosides 3–4

Derivatives of 8-vinyl guanosine, including 8-(2-phenylethenyl)-2′-deoxyguanosine (**3**), were recently reported to be *cis–trans* photoisomerizable switches capable of influencing DNA conformation (39,42–44) Nucleoside **3** photoisomerizes upon irradiation at 370 nm to reach a photostationary E:Z ratio of 6:94, while irradiation at 254 nm caused the reverse photoisomerization and reached a E:Z ratio of 80:20. According to HPLC and NMR analysis, we were able to reproduce these results with nucleoside **3** in our laboratory (42). Replacing the phenyl ring of **3** with a pyridine group generates a new fluorescent nucleoside derivative *trans*-8-(4-pyridyl-vinyl)-2′-deoxyguanosine (**4**) that exhibits little, if any photoswitching (45). This feature allows simplified interpretation of CD and fluorescence data collected using compound **4** in the context of oligonucleotides.

Syn–anti conformational analyses of nucleosides 2–4

Introducing bulky substituents to the C8 position of a purine residue is known to shift the conformational preference of the N9-C1′ glycosidic bond towards *syn* (36–38). This can be evaluated using ^1H and ^{13}C NMR. A conformational change from *anti* to *syn* correlates with a downfield shift of H2′, C1′, C3′ and C4′ and an upfield shift of the C2′ signal (46,47). According to this analysis, the **2PyG** nucleoside **2** prefers a *syn* conformation. In contrast, the C8 vinyl bridged compounds **3** and **4** exhibit chemical shifts consistent with an *anti* conformational preference of the glycosidic bond (Supplementary Table S1). These preferences were confirmed by 2D-ROESY experiments, where strong cross peaks were observed between the phenyl/pyridyl rings and 5′OH, H5′, H3′ and H2′ of compounds **3** and **4**, but were absent in **2PyG** (Supplementary Figures S8–S10). These results confirm a *syn* conformational preference for **2PyG**, and *anti* preference for **StG** and **4PVG**. These conformational preferences might be important in the context of oligonucleotides, where **StG** and **4PVG** are generally less disruptive to DNA folding than **2PyG**.

Global structure and thermal stabilities of oligonucleotides

In K^+-containing solutions, the human telomeric repeat DNA sequence $[G_3(T_2AG_3)_3]$ 'hTelo' can fold into several distinct G-quadruplex conformations in populations that are largely determined by the 5′- and 3′-flanking nucleotides (3,48–50). The sequence studied here ($TT[G_3(T_2AG_3)_3]A$) mostly adopts a '(3+1) parallel–anti-parallel hybrid' topology in the presence of K^+ (49). In Na^+-containing solutions this same sequence folds into a 'anti-parallel' topology in solution (50,51).

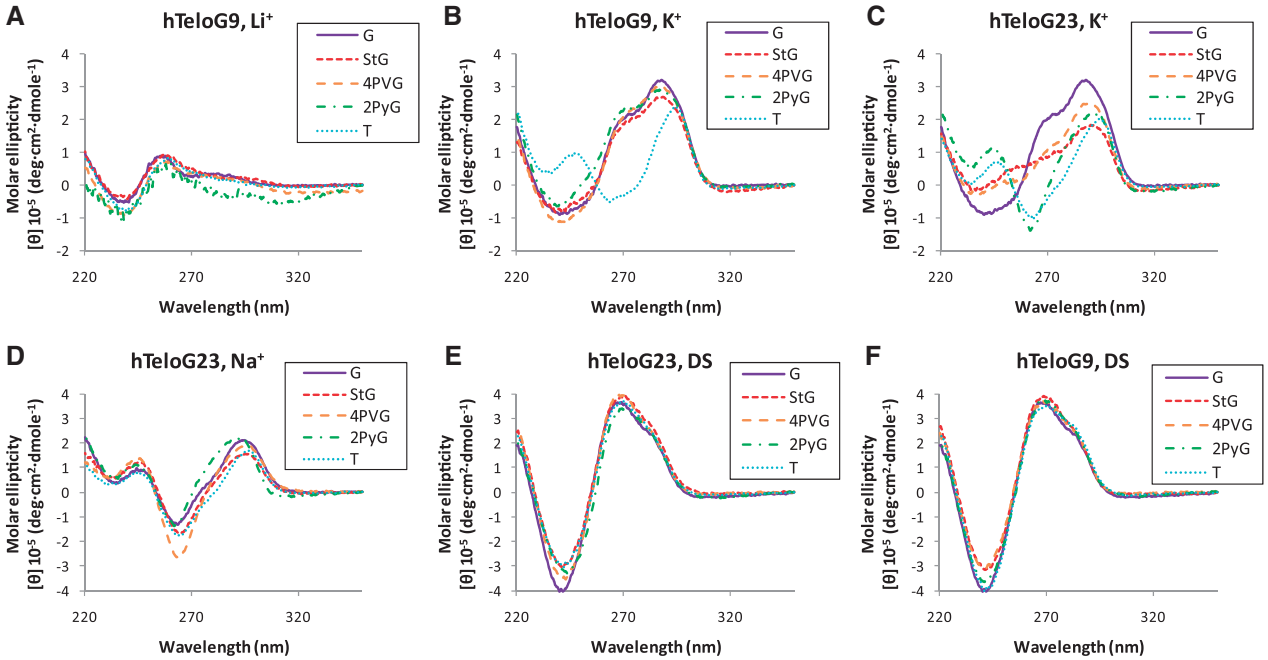

Figure 3. CD spectra of single-stranded hTeloG9 and hTeloG23 derivatives in 100 mM LiCl (**A**), 100 mM KCl (**B** and **C**) or 100 mM NaCl (**D**). Double-stranded DNA samples 'DS' included 1.1 equivalents of the complementary strand and were prepared in 100 mM NaCl (**E** and **F**). All samples contained 2 μM of DNA in an aqueous 10 mM cacodylate buffer (pH 7.4).

Each of these structures contain a characteristic mixture of *syn* and *anti* glycosidic conformations of guanosines involved in G-tetrad formation (3).

Folding of single-stranded hTelo oligonucleotides was controlled by variation of alkali metal salts in the buffer. The global structures and stabilities of the resulting mixtures were assessed using temperature-dependent CD. In Li^+-containing solutions, CD data were consistent with mostly unfolded, G-stacked single-stranded DNA (Figure 3A). Similar results were obtained for all modifications introduced at positions G9 and G23 of hTelo in Li^+ buffer. In buffers containing 100 mM KCl, hTelo adopts a '(3 + 1) hybrid' structure that exhibits a positive CD peak at 288 nm with a shoulder at 270 nm and a minimum at 242 nm (49). The same characteristic CD spectrum was observed when G9 was replaced with **2PyG**, **StG** and **4PVG**, suggesting the presence of wild-type folds (Figure 3B). In K^+ buffers, **2PyG** caused a larger thermal stabilization of the '(3 + 1) hybrid' structure (10°C) as compared to **StG** and **4PVG** (5°C and 8°C, Table 2). In contrast, replacing G9 with T caused very large changes to the global structure of hTelo in K^+ (Figure 3B) that were accompanied by a dramatic decrease in thermal stability ($\Delta T_m = -23$°C, Table 2). We interpret these spectral changes and decreased stability as the loss of one G-tetrad and formation of a G-quadruplex containing only two G-tetrads with 'head-to-head' heteropolar stacking orientation (52). These results suggest that position G9 is sensitive to mutation, and that **2PyG**, **StG** and **4PVG** are incorporated directly into the G-tetrads of natively folded hTelo in the presence of K^+.

The substitution of G23 with **2PyG** caused hTelo to fold into an 'anti-parallel' topology even in K^+ solutions (Figure 3C). This structure, where G23 adopts a syn conformation, is normally only observed in Na^+-containing solutions (50,51). hTeloG23(**2PyG**) was therefore characterized in Na^+ buffer, where it exhibited nearly the same global structure and thermal stability as the wild-type sequence in Na^+ ($\Delta T_m = -2$°C, Figure 3D and Table 2). **StG** and **4PVG**, in contrast, did not force hTeloG23 to fold into an 'anti-parallel' structure in K^+ solutions, and, like the wild-type sequence, two maxima in the region between 270 and 305 nm, and a minimum at ~240 nm were observed (Figure 3C). **StG** and **4PVG** were also compatible with the formation of the 'anti-parallel' hTelo structure in Na^+ solutions (Figure 3D). Taken together, these results suggest that single-stranded hTelo oligonucleotides containing **StG** and **4PVG** exhibit folding behavior more similar to wild-type hTelo than **2PyG** or T-containing variants.

In contrast to the mutation-sensitive folding of single-stranded hTelo, the substitution of position G9 or G23 with **2PyG**, **StG**, **4PVG** or T resulted in little impact on the global structure of the corresponding duplex DNAs (Figure 3E and F). Due to the close proximity of G23 to the end of the oligonucleotide, these modifications had little impact on thermal stability of the duplex (Table 2). Duplexes containing modifications at the central G9 position, in contrast, exhibited thermal stabilities that were highly sensitive to mutations. T incorporation at G9 caused a $\Delta T_m = -8$°C as compared to the wild type hTelo duplex (Table 2). The 8-substituted guanosines caused much less loss in thermal stability than *T*, with

Table 2. Thermal denaturation melting temperatures (T_m) of single-stranded oligonucleotides in K^+ or Na^+, and duplex samples (DSs) in Na^+ as determined by temperature-dependent CD

Name	X	T_m in K^+ (ΔT_m)	T_m in Na^+ (ΔT_m)	T_m of DS (ΔT_m)
hTelowt	G	67.7	53.5	66.0
hTeloG9	**StG**	73.1 (5.4)	60.6 (7.1)	63.0 (−3.0)
	4PVG	75.9 (8.2)	61.1 (7.6)	64.6 (−1.4)
	2PyG	77.5 (9.8)	61.8 (8.3)	61.2 (−4.8)
	T	44.6 (−23)	39.2 (−14)	57.8 (−8.2)
hTeloG23	**StG**	59.5 (−8.2)	52.7 (−0.8)	66.5 (0.5)
	4PVG	61.5 (−6.2)	47.5 (−6.0)	66.9 (0.9)
	2PyG	59.3 (−8.4)	51.6 (−1.9)	66.2 (0.2)
	T	45.2 (−23)	45.1 (−8.4)	64.5 (−1.5)

CD spectra of these same samples are shown in Figure 3. $\Delta T_m = T_m$(modified oligo) − T_m(wild type).

$\Delta T_m = -5°C$, $-3°C$ and $-1°C$ for **2PyG**, **StG** and **4PVG**, respectively (Table 2). Consistent with our results from hTelo G-quadruplexes, these data suggest that duplex oligonucleotides containing **StG** and **4PVG** exhibit duplex-folding equilibria more similar to wild-type hTelo than either **2PyG** or T mutations.

Photophysical properties of 8-substituted guanosines 2–4

2PyG, **StG** and **4PVG**, exhibit large Stoke's shifts (>100 nm) and broad, almost featureless, excitation and emission spectra (Figures 1B and 2 A–C). Due to their larger conjugated π systems, **StG** and **4PVG** are red shifted by 35–75 nm as compared to **2PyG**. The quantum yields of all three nucleosides (**2–4**) approached unity in acetonitrile ($\Phi = 0.57$–0.74), while **2PyG** and **4PVG** exhibited much lower quantum yields in water ($\Phi = 0.02$ and 0.16). Interestingly, **2PyG** and **4PVG** exhibited 2-fold higher quantum yields in D_2O than in H_2O (Figure 1B). **StG**, in contrast, exhibited approximately the same quantum yields in H_2O, D_2O and acetonitrile (Figure 1B). Taken together, these results suggest that water-mediated quenching of **2PyG** and **4PVG** involves proton transfer between photoexcited pyridyl nitrogens and bulk solvent. According to molecular modeling of known structures (49,51), the pyridyl nitrogen of **2PyG** should be partially protected from bulk solvent upon its incorporation into positions G9 and G23 of hTelo. This may explain the higher quantum yields of **2PyG** in the context of G-quadruplex folded DNA (34). The same modeling studies suggest that the pyridyl nitrogen of **4PVG** will remain fully solvated in both quadruplex and duplex DNA. No enhancement in the quantum yield of **4PVG** was therefore predicted upon its incorporation into DNA.

Quantum yields of 8-substituted guanosines in modified oligonucleotides

The vast majority of fluorescent guanosine analogs, such as 2-aminopurine (2AP), 6-methylisoxanthopterin (6-MI) and 3-methylisoxanthopterin (3-MI) are quenched by close proximity and collisions with unmodified purine residues (53,54). These result in large (10–300-fold) decreases in quantum yield upon their incorporation into duplex DNA (55–57). In contrast, 8-substituted guanosines exhibit relatively little, if any quenching upon their incorporation into G-quadruplex, single-stranded or duplex DNA. The quantum yield of **2PyG** in water (0.02) increases to $\Phi = 0.03$–0.05 upon its incorporation into single-stranded or duplex hTelo DNA, and it increases to $\Phi = 0.05$–0.15 when the same oligonucleotides were folded into G-quadruplex structures (34). In the case of **4PVG** ($\Phi = 0.16$), somewhat lower quantum yields were obtained upon its incorporation into single-stranded and quadruplex structures ($\Phi_f = 0.03$–0.07) and still lower quantum yields were observed in the context of duplex DNA ($\Phi_f = 0.02$–0.03). Upon its incorporation into DNA, **StG** exhibited quantum yields that were much higher than both **2PyG** and **4PVG** (Table 1). The values measured for the single-strand and G-quadruplex samples containing **StG** ($\Phi_f = 0.33$–0.45) were higher than the values obtained for duplex DNA ($\Phi_f = 0.20$–0.32). The quantum yields of **StG** are ∼10- to 100-fold higher than all previously reported fluorescent guanine mimics in the context of well-folded nucleic acids with strong base-stacking interactions (53–57).

Energy transfer properties of modified oligonucleotides

The excitation spectra of the oligonucleotides containing 8-substituted guanosines exhibit two maxima corresponding to direct excitation (330–400 nm) and indirect excitation via unmodified nucleobases (260 nm). The ratio of these excitation peaks weighted by the absorbance properties of the DNA and quantum yields of the probe can be used to calculate energy transfer efficiencies (η_t) (34,40,41). Here η_t is defined as the number of photons transferred from active nucleobase energy donors to each energy acceptor, divided by the total number of photons absorbed by all nucleobases at 260 nm. Due to distance and geometry constraints, many of the unmodified nucleobases will be inactive donors, so the reported efficiencies (Table 1) provide a lower limit for the transfer efficiencies of the active donors.

Energy transfer efficiencies from unmodified bases to **2PyG**, **StG** and **4PVG** were ∼2–20-fold higher in G-quadruplexes ($\eta_t = 0.12$–0.36) as compared to the same oligonucleotides in duplex DNA ($\eta_t = 0.02$–0.06). Single-stranded samples in Li^+ exhibited intermediate efficiencies (Table 1). While the calculation of energy transfer efficiencies requires numerous measurements and data processing, a simple comparison of fluorescence intensities resulting from DNA excitation versus selective probe excitation can provide a simple and highly sensitive readout of G-quadruplex formation. According to this approach, the intensity of probe fluorescence upon DNA excitation at 260 nm F(260) is divided by the fluorescence intensity upon selective probe excitation F(X), where X = 325 nm for **2PyG**, 360 nm for **StG** and 375 nm for **4PVG**. Consistent with the trends in energy transfer efficiencies (η_t), duplex DNA exhibited the lowest F(260)/F(X) ratios of 0.9–1.4, single-stranded DNA in Li^+ exhibited intermediate F(260)/F(X) ratios of 1.8–2.3,

while G-quadruplex structures have the highest F(260)/F(X) ratios with 3.0–4.7. These values were similar for all three 8-substituted guanosines, and were independent of the exact structural features and thermal stabilities of the G-quadruplexes or duplexes containing them (Table 1). To evaluate the sensitivity of this F(260)/F(X) ratiometric analysis, serial 2-fold dilutions of hTeloG9 duplex and G-quadruplex DNA containing **StG** were performed (Supplementary Figure S7). The ratios in F(260)/F(X) were concentration independent (quadruplex $\approx$ 4, and duplex $\approx$ 1) and could be readily measured with a standard fluorimeter and sample holder (1-cm path length) using 250 pM solutions of **StG**-labeled DNA (Supplementary Figure S7). This approach therefore provides a simple and highly sensitive fluorescence readout of G-quadruplex folding that is compatible with extremely diluted sample mixtures.

CONCLUSIONS

Fluorescence phenomena enable powerful and readily accessible technologies for probing biomolecule folding and activity (26). Fluorescence-based assays involving fluorescent nucleobase analogs typically assess conformational changes using probes that exhibit lower quantum yields when base-stacked with neighboring residues (58–62). Probes that remain highly emissive when involved in base-stacking interactions will increase the sensitivity of nucleic acid folding studies, and may provide a means to differentiate DNA/RNA folds where alternative base-stacking interactions are present (eg. duplex versus quadruplex). Here, we demonstrate how highly emissive probes that mimic guanine residues can be used to differentiate DNA secondary structures by estimating energy transfer efficiencies between unmodified nucleobases and 8-substituted guanines. To the best of our knowledge, this represents a new paradigm in detecting conformational changes in nucleic acids. While FRET-based studies using large 'external' probes are frequently reported (21), interpretations of the resulting data are limited to changes in probe-to-probe distances, whereas the use of an 'internal' fluorescent base analog can provide a direct readout of the characteristic photophysical properties of secondary structures of nucleic acids containing them. Notably, this can be accomplished by introducing a very small modification (e.g. a single styrene or pyridine group) into the oligonucleotide at a strategic location to provide a highly sensitive and minimally perturbing fluorescent readout of structure.

Polymorphic G-quadruplex structures derived from the human telomeric repeat (hTelo) provide demanding model systems to evaluate internal fluorescent probes for their potential impact on DNA folding and stability. To effectively mimic guanosine in G-quadruplexes, both the Watson–Crick and Hoogsteen hydrogen bonding faces must be maintained. Previous studies have demonstrated that subtle changes to either face (e.g. 7-deazaguanine, 6-thioguanine or inosine) result in large losses in G-quadruplex folding kinetics and stability (63). Indeed, single base mutations (G→T) in hTelo DNA resulted in large losses to intramolecular G-quadruplex thermal stabilities ranging from 8°C to 24°C, while duplexes containing the same mutations lost only from 2°C to 8°C of thermal stability (Table 2). On DNA folding and stability, 8-susbtituted guanosines exhibited context-dependent effects but were generally well-tolerated in both G-quadruplex and duplex oligonucleotides.

2PyG was the first reported example of a fluorescent guanine mimic that exhibits the same or higher quantum yield when base-stacked with neighboring purine residues (34). As a nucleobase analog, however, **2PyG** suffers from some limitations including a *syn* glycosidic conformational preference, a relatively low-quantum yield in water (Φ = 0.02–0.15), and an excitation maximum in the UV. For these reasons, a second generation of 8-substituted-2′-deoxyguanosines with expanded pi-systems was developed. One known derivative, 8-(2-phenylethenyl)-2′-deoxyguanosine (**StG**, Figure 1B) was previously reported to exhibit an *anti* glycosidic conformational preference and the ability to exhibit photoswitching about the vinyl double bond (39,42,44). Here, we report a related derivative 8-[2-(pyrid-4-yl)-ethenyl]-2′-deoxyguanosine (**4PVG**, Figure 1B) that also exhibits a preference for an *anti* glycosidic conformation, but due to the presence of a pyridyl nitrogen atom, it does not act as a photoswitch. As compared to **2PyG**, both of these vinyl-bridged derivatives exhibit red-shifted excitation and emission maxima, lower perturbations of DNA structure/stability, and higher quantum yields. To the best of our knowledge, **StG** displays the highest quantum yield of all reported purine base analogs in the context of folded nucleic acids (Φ = 0.20–0.45). The quantum yield of **StG** is not as environmentally sensitive as **2PyG** and **4PVG**, but it can still report DNA folding due to its ability to serve as an emissive energy acceptor for unmodified nucleobase donors.

Previous studies have suggested that the enhanced quantum yields of unmodified guanine residues upon O^6 ion coordination are responsible for the unusually efficient energy transfer reactions mediated by G-quadruplex structures (34). It was not clear from these results, however, if efficient energy transfer resulted from the intrinsic properties of G-quadruplexes, the unusual photophysical characteristics of **2PyG**, or some combination thereof. Here we report a similar range of transfer efficiencies for all three 8-substitued guanosines evaluated in G-quadruplexes (η_t = 0.12–0.31), suggesting that efficient energy transfer results from the intrinsic properties of G-quadruplex structures, not the probes. In all cases, the energy transfer efficiencies were structure dependent, with η_t(duplex) < η_t(single strand) < η_t(G-quadruplex). In the case of G-quadruplex structures, the combination of efficient energy transfer, high-probe quantum yields, and high molar extinction coefficient of the oligonucleotide ($\varepsilon_{260nm} \approx 250\,000\,cm^{-1}M^{-1}$) results in very bright fluorescence emissions that allow for the detection of G-quadruplex conformations at oligonuclotide concentrations of 250 pM or lower using a standard fluorimeter and sample holder. Even in such dilute solutions, a simple comparison of emission intensities resulting from selective probe excitation versus excitation of the DNA provides a

highly convenient, sensitive and reliable means to characterize the folded states of oligonucleotides. The trends from these ratiometric analyses matched those from detailed analyses of energy transfer efficiencies. In both cases, the trends were independent of the exact structural features of the G-quadruplex or 8-substituted guanosine probe used. Given the simplicity and sensitivity of this approach, we expect that it will be compatible with conformational analyses using fluorescence microscopy and single molecule spectroscopy.

SUPPLEMENTARY DATA

Supplementary Data are available at NAR Online.

ACKNOWLEDGEMENTS

We are grateful to Professor Andrea Vasella, Dr Fabio De Giacomo and Dr Thomas Steinlin for providing 8-substituted guanines for initial fluorescence studies (64).

FUNDING

University of Zürich Forschungskredit (57131901); Swiss National Science Foundation (130074). Funding for open access charge: Swiss Federal Grant.

Conflict of interest statement. None declared.

REFERENCES

1. Franklin,R.E. and Gosling,R.G. (1953) Molecular configuration in sodium thymonucleate. *Nature*, **171**, 740–741.
2. Catasti,P., Chen,X., Mariappan,S.V.S., Bradbury,E.M. and Gupta,G. (1999) DNA repeats in the human genome. *Genetica*, **106**, 15–36.
3. Patel,D.J., Phan,A.T. and Kuryavyi,V. (2007) Human telomere, oncogenic promoter and 5′-UTR G-quadruplexes: Diverse higher order DNA and RNA targets for cancer therapeutics. *Nucleic Acids Res.*, **35**, 7429–7455.
4. Eddy,J. and Maizels,N. (2006) Gene function correlates with potential for G4 DNA formation in the human genome. *Nucleic Acids Res.*, **34**, 3887–3896.
5. Huppert,J.L. and Balasubramanian,S. (2007) G-quadruplexes in promoters throughout the human genome. *Nucleic Acids Res.*, **35**, 406–413.
6. Qin,Y. and Hurley,L.H. (2008) Structures, folding patterns, and functions of intramolecular DNA G-quadruplexes found in eukaryotic promoter regions. *Biochimie*, **90**, 1149–1171.
7. Cahoon,L.A. and Seifert,H.S. (2009) An alternative DNA structure is necessary for pilin antigenic variation in Neisseria gonorrhoeae. *Science*, **325**, 764–767.
8. Hurley,L.H. (2002) DNA and its associated processes as targets for cancer therapy. *Nat. Rev. Cancer*, **2**, 188–200.
9. Mergny,J.L., Riou,J.F., Mailliet,P., Teulade-Fichou,M.P. and Gilson,E. (2002) Natural and pharmacological regulation of telomerase. *Nucleic Acids Res.*, **30**, 839–865.
10. Neidle,S. and Parkinson,G. (2002) Telomere maintenance as a target for anticancer drug discovery. *Nat. Rev. Drug Discov.*, **1**, 383–393.
11. Pennarun,G., Granotier,C., Gauthier,L.R., Gomez,D. and Boussin,F.D. (2005) Apoptosis related to telomere instability and cell cycle alterations in human glioma cells treated by new highly selective G-quadruplex ligands. *Oncogene*, **24**, 2917–2928.
12. Lane,A.N., Chaires,J.B., Gray,R.D. and Trent,J.O. (2008) Stability and kinetics of G-quadruplex structures. *Nucleic Acids Res.*, **36**, 5482–5515.
13. Phan,A.T., Luu,K.N. and Patel,D.J. (2006) Different loop arrangements of intramolecular human telomeric (3+1) G-quadruplexes in K+ solution. *Nucleic Acids Res.*, **34**, 5715–5719.
14. Ambrus,A., Chen,D., Dai,J.X., Jones,R.A. and Yang,D.Z. (2005) Solution structure of the biologically relevant G-quadruplex element in the human c-MYC promoter. implications for g-quadruplex stabilization. *Biochemistry*, **44**, 2048–2058.
15. Phan,A.T., Kuryavyi,V., Burge,S., Neidle,S. and Patel,D.J. (2007) Structure of an unprecedented G-quadruplex scaffold in the human c-kit promoter. *J. Am. Chem. Soc.*, **129**, 4386–4392.
16. Jin,R.Z., Gaffney,B.L., Wang,C., Jones,R.A. and Breslauer,K.J. (1992) Thermodynamics and structure of a DNA tetraplex - a spectroscopic and calorimetric study of the tetramolecular complexes of d(TG_3T) and d($TG_3T_2G_3T$). *Proc. Natl Acad. Sci. USA*, **89**, 8832–8836.
17. Mergny,J.L., Phan,A.T. and Lacroix,L. (1998) Following G-quartet formation by UV-spectroscopy. *FEBS Lett.*, **435**, 74–78.
18. Phan,A.T. and Mergny,J.L. (2002) Human telomeric DNA: G-quadruplex, i-motif and watson-crick double helix. *Nucleic Acids Res.*, **30**, 4618–4625.
19. Parkinson,G.N., Lee,M.P.H. and Neidle,S. (2002) Crystal structure of parallel quadruplexes from human telomeric DNA. *Nature*, **417**, 876–880.
20. He,F., Tang,Y.L., Wang,S., Li,Y.L. and Zhu,D.B. (2005) Fluorescent amplifying recognition for DNA G-quadruplex folding with a cationic conjugated polymer: A platform for homogeneous potassium detection. *J. Am. Chem. Soc.*, **127**, 12343–12346.
21. Mergny,J.L. and Maurizot,J.C. (2001) Fluorescence resonance energy transfer as a probe for G-quartet formation by a telomeric repeat. *Chembiochem*, **2**, 124–132.
22. Nagatoishi,S., Nojima,T., Galezowska,E., Juskowiak,B. and Takenaka,S. (2006) G quadruplex-based FRET probes with the thrombin-binding aptamer (TBA) sequence designed for the efficient fluorometric detection of the potassium ion. *Chembiochem*, **7**, 1730–1737.
23. Schaffitzel,C., Berger,I., Postberg,J., Hanes,J., Lipps,H.J. and Pluckthun,A. (2001) In vitro generated antibodies specific for telomeric guanine-quadruplex DNA react with Stylonychia lemnae macronuclei. *Proc. Natl Acad. Sci. USA*, **98**, 8572–8577.
24. Alzeer,J. and Luedtke,N.W. (2010) pH-mediated fluorescence and G-quadruplex binding of amido phthalocyanines. *Biochemistry*, **49**, 4339–4348.
25. Moreira,B.G., You,Y., Behlke,M.A. and Owczarzy,R. (2005) Effects of fluorescent dyes, quenchers, and dangling ends on DNA duplex stability. *Biochem. Biophys. Res. Commun.*, **327**, 473–484.
26. Sinkeldam,R.W., Greco,N.J. and Tor,Y. (2010) Fluorescent analogs of biomolecular building blocks: design, properties, and applications. *Chem. Rev.*, **110**, 2579–2619.
27. Wilhelmsson,L.M. (2010) Fluorescent nucleic acid base analogues. *Q. Rev. Biophys.*, **43**, 159–183.
28. Srivatsan,S.G., Weizman,H. and Tor,Y. (2008) A highly fluorescent nucleoside analog based on thieno[3,4-d] pyrimidine senses mismatched pairing. *Org. Biomol. Chem.*, **6**, 1334–1338.
29. Rist,M.J. and Marino,J.P. (2002) Fluorescent nucleotide base analogs as probes of nucleic acid structure, dynamics and interactions. *Cur. Org. Chem.*, **6**, 775–793.
30. Firth,A.G., Fairlamb,I.J.S., Darley,K. and Baumann,C.G. (2006) Sonogashira alkynylation of unprotected 8-brominated adenosines and guanosines: fluorescence properties of compact conjugated acetylenes containing a purine ring. *Tetrahedron Lett.*, **47**, 3529–3533.
31. Greco,N.J. and Tor,Y. (2007) Furan decorated nucleoside analogues as fluorescent probes: synthesis, photophysical evaluation, and site-specific incorporation. *Tetrahedron*, **63**, 3515–3527.
32. Wanninger-Weiss,C., Valis,L. and Wagenknecht,H.A. (2008) Pyrene-modified guanosine as fluorescent probe for DNA modulated by charge transfer. *Bioorgan. Med. Chem.*, **16**, 100–106.

33. Butler,R.S., Cohn,P., Tenzel,P., Abboud,K.A. and Castellano,R.K. (2009) Synthesis, photophysical behavior, and electronic structure of push-pull purines. *J. Am. Chem. Soc.*, **131**, 623–633.
34. Dumas,A. and Luedtke,N.W. (2010) Cation-mediated energy transfer in G-quadruplexes revealed by an internal fluorescent probe. *J. Am. Chem. Soc.*, **132**, 18004–18007.
35. Gaied,N.B., Glasser,N., Ramalanjaona,N., Beltz,H., Wolff,P., Marquet,R., Burger,A. and Mely,Y. (2005) 8-vinyl-deoxyadenosine, an alternative fluorescent nucleoside analog to 2′-deoxyribosyl-2-aminopurine with improved properties. *Nucleic Acids Res.*, **33**, 1031–1039.
36. Birnbaum,G.I., Lassota,P. and Shugar,D. (1984) 8-Chloroguanosine - solid-state and solution conformations and their biological implications. *Biochemistry*, **23**, 5048–5053.
37. Dias,E., Battiste,J.L. and Williamson,J.R. (1994) Chemical probe for glycosidic conformation in telomeric Dnas. *J. Am. Chem. Soc.*, **116**, 4479–4480.
38. Xu,Y. and Sugiyama,H. (2006) Formation of the G-quadruplex and i-motif structures in retinoblastoma susceptibility genes (Rb). *Nucleic Acids Res.*, **34**, 949–954.
39. Ogasawara,S. and Maeda,M. (2008) Straightforward and reversible photoregulation of hybridization by using a photochromic nucleoside. *Angew. Chem. Int. Edit.*, **47**, 8839–8842.
40. Xu,D.G. and Nordlund,T.M. (2000) Sequence dependence of energy transfer in DNA oligonucleotides. *Biophys. J.*, **78**, 1042–1058.
41. Nordlund,T.M. (2007) Sequence, structure and energy transfer in DNA. *Photochem. Photobiol.*, **83**, 625–636.
42. Ogasawara,S., Saito,I. and Maeda,M. (2008) Synthesis and reversible photoisomerization of photoswitchable nucleoside, 8-styryl-2′-deoxyguanosine. *Tetrahedron Lett.*, **49**, 2479–2482.
43. Saito,Y., Matsumoto,K., Takeuchi,Y., Bag,S.S., Kodate,S., Morii,T. and Saito,I. (2009) Fluorescence switching of photochromic vinylpyrene-substituted 2′-deoxyguanosine. *Tetrahedron Lett.*, **50**, 1403–1406.
44. Ogasawara,S. and Maeda,M. (2009) Reversible photoswitching of a G-quadruplex. *Angew. Chem. Int. Edit.*, **48**, 6671–6674.
45. Upon extensive irradiation of **4PVG** at 370 nm, a maximum of 24% of the Z form was observed in solution at room temperature.
46. Uesugi,S. and Ikehara,M. (1977) C-13 Magnetic-resonance spectra of 8-substituted purine nucleosides - characteristics shifts for syn conformation. *J. Am. Chem. Soc.*, **99**, 3250–3253.
47. Stolarski,R., Hagberg,C.E. and Shugar,D. (1984) Studies on the dynamic syn-anti equilibrium in purine nucleosides and nucleotides with the aid of H-1 and C-13 NMR-spectroscopy. *Eur. J. Biochem.*, **138**, 187–192.
48. Lim,K.W., Amrane,S., Bouaziz,S., Xu,W., Mu,Y., Patel,D.J., Luu,K.N. and Phan,A.T. (2009) Structure of the human telomere in K+ solution: a stable basket-type G-quadruplex with only two G-tetrad layers. *J. Am. Chem. Soc.*, **131**, 4301–4309.
49. Luu,K.N., Phan,A.T., Kuryavyi,V., Lacroix,L. and Patel,D.J. (2006) Structure of the human telomere in K+ solution: an intramolecular (3 + 1) G-quadruplex scaffold. *J. Am. Chem. Soc.*, **128**, 9963–9970.
50. Li,J., Correia,J.J., Wang,L., Trent,J.O. and Chaires,J.B. (2005) Not so crystal clear: the structure of the human telomere G-quadruplex in solution differs from that present in a crystal. *Nucleic Acids Res.*, **33**, 4649–4659.
51. Wang,Y. and Patel,D.J. (1993) Solution structure of the human telomeric repeat d[AG(3)(T(2)AG(3))3] G-tetraplex. *Structure*, **1**, 263–282.
52. Masiero,S., Trotta,R., Pieraccini,S., De Tito,S., Perone,R., Randazzo,A. and Spada,G.P. (2010) A non-empirical chromophoric interpretation of CD spectra of DNA G-quadruplex structures. *Org. Biomol. Chem.*, **8**, 2683–2692.
53. Narayanan,M., Kodali,G., Xing,Y. and Stanley,R.J. (2010) Photoinduced electron transfer occurs between 2-aminopurine and the DNA nucleic acid monophosphates: results from cyclic voltammetry and fluorescence quenching. *J. Phys. Chem. B*, **114**, 10573–10580.
54. Narayanan,M., Kodali,G., Xing,Y., Hawkins,M.E. and Stanley,R.J. (2010) Differential fluorescence quenching of fluorescent nucleic acid base analogues by native nucleic acid monophosphates. *J. Phys. Chem. B*, **114**, 5953–5963.
55. Kelley,S.O. and Barton,J.K. (1999) Electron transfer between bases in double helical DNA. *Science*, **283**, 375–381.
56. Hawkins,M.E. (2001) Fluorescent pteridine nucleoside analogs: a window on DNA interactions. *Cell Biochem. Biophys.*, **34**, 257–281.
57. Hawkins,M.E., Pfleiderer,W., Balis,F.M., Porter,D. and Knutson,J.R. (1997) Fluorescence properties of pteridine nucleoside analogs as monomers and incorporated into oligonucleotides. *Anal. Biochem.*, **244**, 86–95.
58. Hawkins,M.E., Pfleiderer,W., Mazumder,A., Pommier,Y.G. and Balis,F.M. (1995) Incorporation of a fluorescent guanosine analog into oligonucleotides and its application to a real time assay for the HIV-1 integrase 3′-processing reaction. *Nucleic Acids Res.*, **23**, 2872–2880.
59. Kimura,T., Kawai,K., Fujitsuka,M. and Majima,T. (2007) Monitoring G-quadruplex structures and G-quadruplex-ligand complex using 2-aminopurine modified oligonucleotides. *Tetrahedron*, **63**, 3585–3590.
60. Gray,R.D., Petraccone,L., Trent,J.O. and Chaires,J.B. (2010) Characterization of a K(+)-induced conformational switch in a human telomeric DNA oligonucleotide using 2-aminopurine fluorescence. *Biochemistry*, **49**, 179–194.
61. Kirk,S.R., Luedtke,N.W. and Tor,Y. (2001) 2-Aminopurine as a real-time probe of enzymatic cleavage and inhibition of hammerhead ribozymes. *Bioorgan. Med. Chem.*, **9**, 2295–2301.
62. Hawkins,M.E. (2008) Fluorescent pteridine probes for nucleic acid analysis. *Method Enzymol.*, **450**, 201–231.
63. Gros,J., Rosu,F., Amrane,S., De Cian,A., Gabelica,V., Lacroix,L. and Mergny,J.L. (2007) Guanines are a quartet's best friend: impact of base substitutions on the kinetics and stability of tetramolecular quadruplexes. *Nucleic Acids Res.*, **35**, 3064–3075.
64. Xu,M., De Giacomo,F., Paterson,D.E., George,T.G. and Vasella,A. (2003) An improved procedure for the preparation of 8-substituted guanines. *Chem. Commun.*, **12**, 1452–1453.